AUTOMATIC HUMAN FALL DETECTION IN FRACTIONAL FOURIER DOMAIN FOR ASSISTED LIVING

Shengheng Liu[1,2,3]*, Zhengxin Zeng*[1,2]*, Yimin D. Zhang*[3]*, Tingting Fan*[1,2]*, Tao Shan*[1,2,*]*, and Ran Tao*[1,2]

[1]School of Information and Electronics, Beijing Institute of Technology, Beijing, P. R. China
[2]Beijing Key Laboratory of Fractional Signals and Systems, Beijing, P. R. China
[3]Department of Electrical and Computer Engineering, Temple University, Philadelphia, PA, USA
[*]shantao@bit.edu.cn

ABSTRACT

Fast and accurate detection of elderly falls can significantly reduce the rate of morbidity and mortality. In the past decade, extensive research has been performed to achieve real-time fall monitoring solutions. In this paper, we consider the radar-based modality and utilize the family of fractional Fourier transform to enhance the motion Doppler signature of falls. Compare with the conventional time-frequency analysis approaches, the proposed method achieves higher signal energy concentration and thus yields improved fall detection in low signal-to-noise ratio scenarios. Experimental results are used to validate the theoretical analysis and to demonstrate the feasibility of the proposed approach.

Index Terms— Radar Doppler spectrogram, fractional Fourier transform, short-time Fourier transform, fall detection, biomedical signal processing

1. INTRODUCTION

As a widely recognized major public health problem, elderly falls can cause a variety of severe physical and psychological consequences [1, 2]. Prompt attention with minimal time delay between the fall event and medical treatment is critical to save the patients' lives. Thus it has attracted significantly increased interest in both industry and research communities, and several real-time monitoring approaches have been developed over the last a few years. Those approaches include active involvements (e.g. pressing a button) [3], wearable accelerometer/gyroscope sensors [4, 5], floor vibration and sound sensors [6], infrared detectors [7], video sensors [8] and radar [9–14].

Among all the noninvasive fall monitoring techniques, the radar technology is uniquely suitable due to its applicability to all types of lighting conditions with less "false positives". In [9–12], fall detection was performed using a support vector machine (SVM) classifier [13], while in [14], sparse Bayesian classifier was used, which is superior to the SVM because fewer relevance vectors can be used. Prior to the detections, all these schemes applied short-time Fourier transform (STFT) to the raw date collected from the radar receiver to acquire the spectrograms. Time-scale analysis based wavelets are also reported in [15, 16].

This work was supported in part by the National Natural Science Foundation of China under grants Nos. 61172176, 61331021 and 61421001. Financial support from the China Scholarship Council for S. Liu's stay at Temple University (No. [2015]3022) is also gratefully acknowledged.

Fall and other human gaits generate time-varying Doppler and micro-Doppler signatures which, over a short time period, can be well approximated as a linear frequency modulation (LFM) signal, which is also commonly referred to as a chirp. For various falls and other events, the Doppler and micro-Doppler frequencies change rapidly and, as such, conventional STFT suffers from a limited frequency resolution and poor power concentration. As a result, fall detection performance would degrade, particularly when the input signal-to-noise ratio (SNR) is low. One promising solution is to apply the family of fractional Fourier transform (FrFT) [17]. As FrFT projects signals onto chirp bases, it exhibits superior capability to concentrate energy for signals approximately characterizable by LFM. In addition, unlike the bilinear time-frequency (TF) representations, the FrFT does not suffer form the effect of cross-term interference. The FrFT approach can be defined over a finite time window, known as the short-time fractional Fourier transform (STFrFT) [18], which has found applications in chirp signal separation [19], synthetic aperture radar image autofocusing [20], and extraction of marine target micro-Doppler signatures [21].

In this paper, we exploit the FrFT and STFrFT concepts to develop an effective elderly fall detection approach defined in the fractional Fourier domain (FrFD). An FrFT-based threshold decision method is developed, and FrFD features obtained from the STFrFT-based spectrogram are chosen to classify the fall and non-fall events. The high concentration of the FrFD spectrum enables improved detection and the classification capability in low SNR situations. The novelty of our approach lies in performing both detection and classification in the time-fractional Fourier domain rather than in the commonly used time-frequency domain.

The remainder of this paper is organized as follows. An overview of FrFT and STFrFT, and an introduction of the signal model are provided in Section 2. The proposed method is presented in Section 3. The experimental setup and the analysis of the real data processing is given in Section 4. Conclusion is drawn in Section 5.

2. SIGNAL MODEL

In our study, the transmitted waveform is an LFM continuous-wave (LFMCW), as shown in Fig. 1. The continuous-time waveform transmitted over the nth pulse period is given by

$$s_t(t) = \sum_{n=0}^{\infty} A_t \mathrm{e}^{\mathrm{j}\left[2\pi\left(f_c-\frac{B}{2}\right)t+\pi\mu((t-(n-1))T)^2+\varphi_0\right]}, \qquad (1)$$

for $(n-1)T \le t < T$, where A_t stands for the transmitted signal amplitude, f_c represents the center frequency, B and T respectively

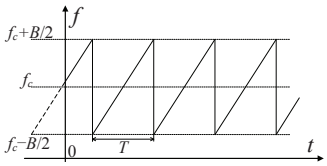

Fig. 1. Instantaneous frequency of an LFMCW signal.

denote the sweep bandwidth and sweep time, $\mu = B/T$ is the chirp rate, and φ_0 is the initial phase at time $t = 0$.

The radar return from a point target is generally a time-delayed and scaled replica of the transmitted signal. Thus, consider a point target σ which is located at a distance of R_0 from the radar at time instant t_0, and moves with a velocity of $v(t)$ towards a direction which forms an angle of θ between the radar direction. As such, the radar echo signal corresponding to the point target is given by [14]

$$s_r(t;\sigma) = A_r s_t\left(t - \frac{2R_0 + 2\int_{t_0}^{t} v(t)\cos\theta \mathrm{d}t}{\mathrm{c}}\right) + w(t), \quad (2)$$

where A_r denotes the target reflection coefficient, c is the light velocity, and $w(t)$ represents additive white Gaussian noise.

The human body return can be regarded as the superposition of returns from a finite number of point targets located over the body region Ω_A. Therefore, the return signal is the integration over the region Ω_A, which can be represented as [14]

$$\hat{s}_r(t) = \int_{\sigma\in\Omega_A} s_r(t;\sigma)\mathrm{d}\sigma. \quad (3)$$

3. PROPOSED METHOD

3.1. Overview of FrFT and STFrFT

We first briefly summarize the FrFT and the STFrFT methods which are used to develop the proposed work.

The mathematical definition of the pth-order continuous FrFT [17] is given in (4), shown on the bottom of this page, where $\alpha = p\pi/2$ is the fractional rotation angle, p is the order value, u denotes the FrFD frequency, and D is an integer. Note that p can take an arbitrary real value, and the classical Fourier transform corresponds to the case of $p = 1$. For a certain chirp frequency modulation rate μ, if $\alpha = \operatorname{arc\,cot}(-2\pi\mu)$, the signal energy will be concentrated in the FrFD. The STFrFT is defined by multiplying the input signal $x(t)$ with a window $g(t)$ before computing the FrFT [18], i.e.,

$$\{\mathrm{STFrFT}_p x\}(t,u) = \int_{-\infty}^{\infty} g(\tau - t)K_\alpha(\tau,u)x(\tau)\mathrm{d}\tau, \quad (5)$$

where $K_\alpha(\tau,u)x(\tau)$ is implicitly defined in (4).

The STFrFT uses a fixed time window to perform FrFT of the signal over a certain length of time samples. The window size trades off between the time resolution and frequency resolution. By computing the STFrFT in a sliding window manner, the instantaneous FrFD spectrum over the entire time period can be obtained.

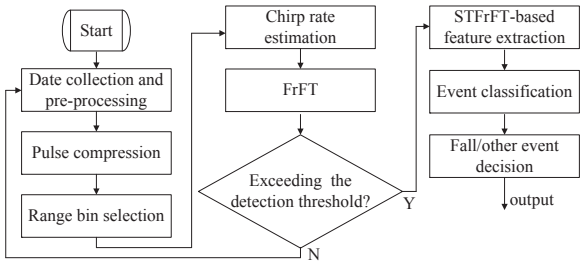

Fig. 2. Proposed human fall detection scheme.

3.2. Signal Representation in the Fractional Fourier Domain

The diagram of the proposed method is depicted in Fig. 2. The first step is pre-processing of the collected raw data such as data format conversion, direct current extraction, and data matrix reshape.

The $(m,\tilde{n})$th element of the reshaped data matrix, $\tilde{\mathbf{s}}_r$, is obtained from the received data $\hat{s}_r(n)$ as

$$[\tilde{\mathbf{s}}_r]_{(m,\tilde{n})} = s_r\left((m-1)N_p + \tilde{n}\right), \quad (6)$$

where $m = 1,2,\ldots,M_p$ and $\tilde{n} = 1,2,\ldots,N_p$ are the slow and fast time indices, with M_p and N_p respectively denoting the number of slow-time pulses and the number of fast-time samples per pulse. Pulse compression is then performed to the reshaped data matrix over the fast-time samples, where the range data is interpolated with a factor of two. The range-pulse figure,represented by a $(2N_p)\times M_p$ matrix $\mathbf{S}_r$, can then be obtained through the following fast Fourier transform (FFT) to identify range bins in which strong target echoes are present:

$$\mathbf{S}_r = \mathrm{FFT}\left\{\left[\tilde{\mathbf{s}}_r \cdot \mathbf{w}_{M_p\times N_p}, \mathbf{0}_{M_p\times N_p}\right]^{\mathrm{T}}\right\}, \quad (7)$$

where $\mathbf{w}$ represents a Hanning window, and $\mathbf{0}_{M_p\times N_p}$ is the $M_p \times N_p$ matrix with all zero elements. Based on this result, further signal processing is applied to ranges with a high energy, representing possible events to be analyzed. The chirp rate of the signal is estimated by using discrete polynomial-phase transform (DPT)-FrFT [22]. Alternatively, when the signal has a long length ($M_p > 2^{12}$), the segmented DPT-sparse discrete fractional Fourier transform (SDFrFT) [23] can be used for fast computation.

Because elderly falls may be accompanied by motions in other body parts and/or cluttered by possible motion of other objects, the signal should be generally characterized with a multi-component time-varying spectrum. Consider a range bin b_t, the estimated chirp rate, $\hat{\mu}_k$, of the kth signal component in the presence of K components is obtained from [22]

$$\hat{\mu}_k = \frac{1}{\tau L_s \Delta t}\arg\max_{f_k}\left|\mathrm{DPT}_2\{\tilde{S}(p,\hat{m}),f,\tau\}\right|, \quad (8)$$

for $k = 1,2,\ldots,K$, where $\mathrm{DPT}_2\{\cdot,f,\tau\}$ denotes the order-two DPT operation, τ is a positive integer, f is the frequency-domain

$$\{\mathrm{FrFT}_p x\}(u) = \int_{-\infty}^{\infty} K_\alpha(u,t)x(t)\mathrm{d}t = \begin{cases} \sqrt{\dfrac{1-\mathrm{j}\cot\alpha}{2\pi}}\displaystyle\int_{-\infty}^{\infty} \mathrm{e}^{\mathrm{j}\frac{t^2+u^2}{2}\cot\alpha - \mathrm{j}tu\csc\alpha}\cdot x(t)\mathrm{d}t, & \alpha \neq D\pi, \\ x(t), & \alpha = 2D\pi, \\ x(-t), & \alpha = (2D\pm 1)\pi, \end{cases} \quad (4)$$

index, and Δt denotes the sampling interval. In addition,

$$\tilde{S}(p,\hat{m}) = \sum_{l=1}^{L_s} \mathbf{S}_r(b_t,(p-1)\cdot L_s + l)\mathrm{e}^{-\mathrm{j}2\pi\hat{m}l/L_s}, \quad (9)$$

where $l = 1,2,\ldots,L_s, \hat{m} = 1,2,\ldots,L_s$, and $p = 1,2,\ldots,P_s$, with P_s denoting the number of segments, L_s the number of samples per segment, and $M_p = L_s P_s$.

To obtain high-resolution and cross-term-free TF representations, the FrFT/SDFrFT methods are then applied to $\mathbf{S}_r(b_t,:)_{1\times M_p}$. To obtain a finer estimation, an exhaustive search near the confirmed chirp rates within the $\pm 5\Delta\mu$ range is conducted, where the step size is given as $\Delta\mu = (2/(M_p N_p \Delta t))^2$ [23]. In [9], the energy burst curve (which is also referred to as the power burst curve in [14]) of the signal was used to detect an event and initiate the classification process. The idea behind it is to identify the signal power presence in a low but non-zero frequency band where human activities can be detected whereas the effect of stationary clutter is excluded. When the signals are represented in the FrFD, this becomes equivalent to examine whether an FrFD spectral line with the zero fractional frequency exceeds the detection threshold. A positive result will ignite the motion classification procedure. Note that, because the radical acceleration of human fall motion is unlikely to exceed the free fall acceleration g=9.8 m/s^2, the corresponding chirp rate can be considered up bounded.

3.3. Fall Detection based on Bayesian Classifier

The main task of the classifier is to distinguish between fall and non-fall events. For classification of human activities, especially fall and non-fall events, a number features have been used [6, 13, 14]. These features include the peak Doppler, offset of the total Doppler, total Doppler bandwidth, standard deviation of the Doppler signal strength, extreme Doppler ratio, and period of the event. In this paper, we consider the following temporal and spectral features that bear the same spirit but are more feasible for the STFrFT-based analysis: Period T (same as the Length of Event in [14]), Chirp rate μ (corresponds to the Extreme Frequency Magnitude in [14]), and FrFD bandwidth B. Note that the FrFD bandwidth is descriptive because the FrFD spectrum of fall events are concentrated, whereas that of non-fall events are not.

The input of the Bayesian classifier, observation vector $\mathbf{z}_n$, contains the extracted values of the selected features from the STFrFT-based spectrogram, i.e.,

$$\mathbf{z}_n = [\hat{T}_n, \hat{\mu}_n, \hat{B}_n]^T \in \mathcal{R}^3, \quad (10)$$

where subscript n is used to underscore event n. The decision rule classifies $\mathbf{z}_n$ to the class $\omega(\mathbf{z}_n)$ that has the highest *a posteriori* probability between the two classes, fall class ω_1 and non-fall class ω_2, as

$$\omega(\mathbf{z}_n) = \arg\max_{\omega\in\{\omega_1,\omega_2\}} \{P(\omega|\mathbf{z}_n)\}, \quad (11)$$

where $P(\omega|\mathbf{z}_n)$ is the *a posteriori* probability. The data set $\mathbf{z}_n$ generally follows the Gaussian distribution [6, 14]. Denote the mean vector and the covariance matrix of the kth class ($k = 1, 2$), as ξ_k and $\mathbf{C}_k$, respectively. Then, the conditional density function is [6]

$$p(\mathbf{z}_n|\omega_k) = \frac{1}{\sqrt{(2\pi)^3|\mathbf{C}_k|}}\mathrm{e}^{-\frac{1}{2}(\mathbf{z}_n-\xi_k)^{\mathrm{T}}\mathbf{C}_k^{-1}(\mathbf{z}_n-\xi_k)}, \quad (12)$$

where $(\cdot)^{\mathrm{T}}$ denote transpose, and $|\mathbf{C}|$ stands for the determination of matrix $\mathbf{C}$. The Bayesian decision rule of the adopted quadratic classifier [6] is given by $\omega(\mathbf{z}_n) = \omega_i$ with

$$i = \arg\max_{k=1,2}\left\{-\frac{1}{2}\ln|\mathbf{C}_k| - \frac{1}{2}(\mathbf{z}_n-\xi_k)^{\mathrm{T}}\mathbf{C}_k^{-1}(\mathbf{z}_n-\xi_k)\right\}. \quad (13)$$

(13) chooses class ω_i for a specific vector $\mathbf{z}_n$ in the three-dimensional (3D) feature space under the maximum *a posteriori* (MAP) criterion.

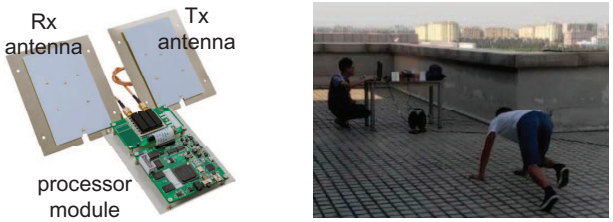

(a) Data collection module

(b) Experiment scene

Fig. 3. Illustration of experimental setup.

4. EXPERIMENT SETUP AND RESULT ANALYSIS

4.1. Experimental setup

In the experiment, an ANCORTEK$^{\mathrm{TM}}$ SDR-KIT 580 module [24] is used for radar data collection. It is a software-defined transmitter-receiver system and can be controlled by graphic user interface installed on a laptop computer. The SDR-KIT 580 module and the experiment scene are shown in Fig. 3.

For transmitted waveform shown in Fig. 1, the echo signal is mixed with the transmitted signal to perform de-chirp process. The center frequency f_c, sampling rate f_s, and sweep bandwidth B are set as 5.8 GHz, 130 KHz, and 100 MHz, respectively. The sweep time T is 0.9830 ms, yielding a slow-time pulse repetition frequency of 1017 Hz. In the TF analysis, a 203-point Hanning window is applied to the slow-time samples. The radial range between the experimental subject and the radar varies between 2 and 11 meters.

We conducted experiments with four different motion patterns, including walking, running, deep squat, and falling. The first three motion patterns are collectively considered as non-fall events. Each of these motion patterns are repeated for ten times by different laboratory assistants. The fall events are repeated for 30 times. As such, a total number of 60 data sets are collected. Half of those data sets are included for training, and the other half data sets are used for classification.

4.2. Experiment results and discussion

To demonstrate the advantage of the proposed FrFD-based approach, the signal spectra and TF representations of the experimental data are illustrated in Fig. 4. A notable zero-frequency (direct current, DC) component with a Doppler modulation in the adjacent region is observed in Figs. 4(a) and 4(d). The results after the DC component removal are shown in Figs. 4(b) and 4(e). It can be estimated from Fig. 4(e) that a fall event occurs at $t = 1.3$ s and lasts about 0.64 s. The fact that the Doppler frequency varies from the DC to about 80 Hz indicates that the subject falls towards the radar. The estimated radical acceleration was about 2.07 m/s^2, which coincides well with the experimental facts. In Figs. 4(c) and 4(f), the FrFT/STFrFT methods were applied to the DC-removed data, and the target spike

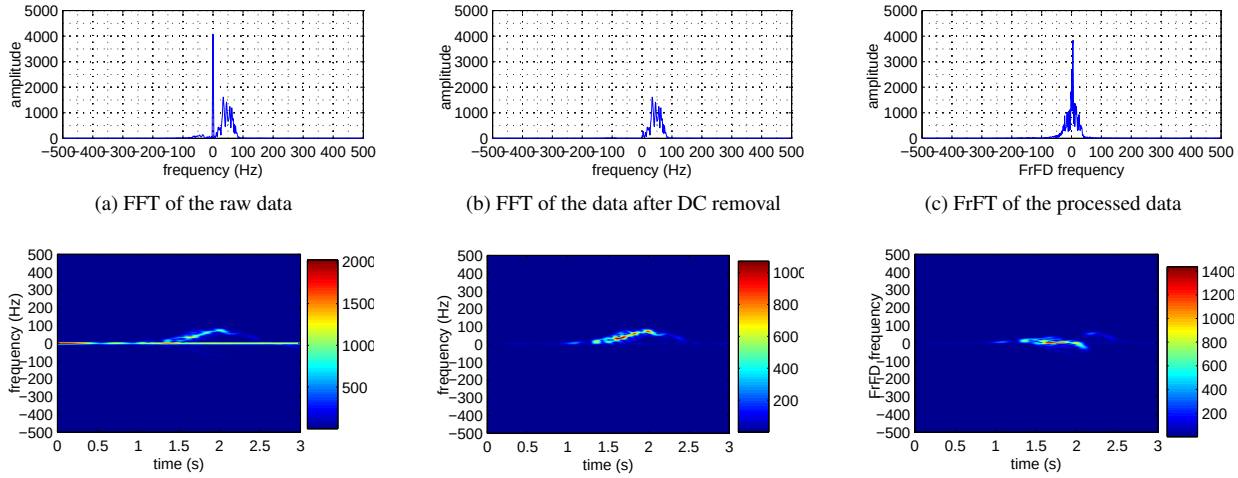

(a) FFT of the raw data (b) FFT of the data after DC removal (c) FrFT of the processed data

(d) STFT of the raw data (e) STFT of the processed data (f) STFrFT of the processed data

Fig. 4. Experiment results.

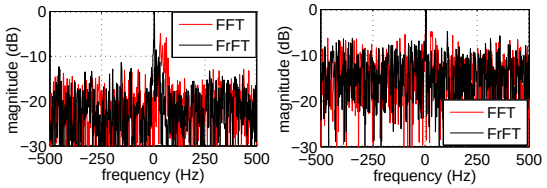

(a) Input SNR=−10 dB (b) Input SNR=−18 dB

Fig. 5. Performance comparison between FFT and FrFT based algorithms with different input SNRs.

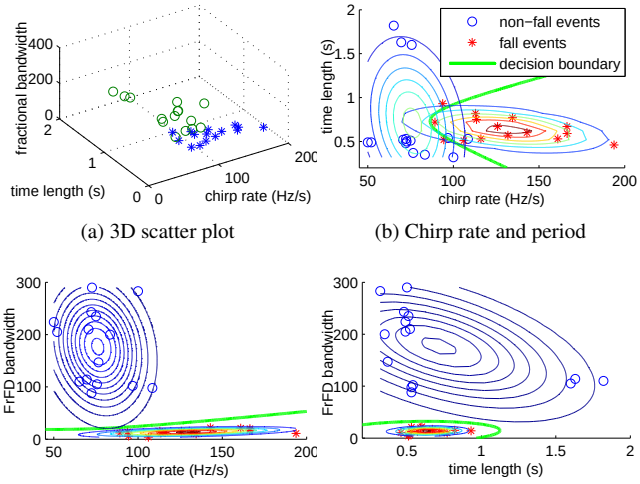

(a) 3D scatter plot (b) Chirp rate and period

(c) Chirp rate and bandwidth (d) Period and bandwidth

Fig. 6. 3D scatter plot and the projection of the training feature vectors on different 2D space.

in Fig. 4(c) is increased by a factor of 2.5. Therefore, a better detection capability in low SNR case is expected.

To verify this fact, white Gaussian noise is added to the raw data collected in the experiments, and the results are depicted in Fig. 5. In the −10 dB SNR case, the result of the FrFT-based method is 5.1 dB higher than that of the FFT-based method. On the other hand, when the SNR is −18 dB, the fall-induced spike using the FFT-based method becomes invisible, whereas the output SNR of the FrFT-based method remains a high level of 9.5 dB and thus enables reliable fall detection.

By utilizing the Bayesian classifier descried in (13), we compute the decision boundaries between the two classification models. Fig. 6 shows the training results of the three features defined in (10). It is seen from Fig. 6(b) that the fall events have higher chirp rates and fixed time lengths of around 0.7 s, whereas it is observed from Fig. 6(c) that the FrFD bandwidths of the fall events are much better concentrated near zero region.

Table 1 provides the confusion matrices of all the data sets being tested. The first three results are computed using the three 2D spaces in the same order as Figs. 6 (b)-(d), while the last result is computed using the 3D space, and all these results are separated by slashes. The test result shows that while any 2D feature space does not provide a perfect distinction, the fall and non-fall events are well separated in the 3D space for classification, which clearly demonstrating the effectiveness of the proposed FrFD automatic human fall detection scheme.

Table 1. Confusion Matrices

Real type	Classification result	
	fall events	non-fall events
fall events	14/14/12/15	1/1/3/0
non-fall events	3/0/0/0	12/15/15/15

5. CONCLUSION

A novel radar fall detection scheme was proposed for assisted living and elderly fall detection. Different from existing time-frequency domain methods, it is the first time to address this problem in the fractional Fourier domain, where an FrFT-based threshold decision triggers the classification procedure and an STFrFT-based feature extraction facilitates the classification. Experiment results confirmed that the proposed scheme can achieve an enhanced detection performance, especially in low SNR cases.

6. REFERENCES

[1] AARP, *Health Innovation Frontiers: Untapped Market Opportunities for the 50+*, Available at http://health50.org/health-innovation-frontiers/.

[2] S. Sadigh, A. Reimers, R. Andersson, and L. Laflamme, "Falls and fall related injuries among the elderly: A survey of residential-care facilities in a Swedish municipality," *Journal of Community Health*, vol. 29, no. 2, pp. 129–140, April 2004.

[3] F.G. Miskelly, "Assistive technology in elderly care," *Age and Ageing*, vol. 30, no. 6, pp. 455–458, November 2001.

[4] A.K. Bourke, J.V. O'Brienb, and G.M. Lyons, "Evaluation of a threshold-based tri-axial accelerometer fall detection algorithm," *Gait & Posture*, vol. 26, no. 2, pp. 194–199, July 2007.

[5] M. Kangas, A. Konttila, P. Lindgren, I. Winblad, and T. Jämsä, "Comparison of low-complexity fall detection algorithms for body attached accelerometers," *Gait & Posture*, vol. 28, no. 2, pp. 285–291, August 2008.

[6] Y. Zigel, D. Litvak, and I. Gannot, "A method for automatic fall detection of elderly people using floor vibrations and sound — Proof of concept on human mimicking doll falls," *IEEE Transactions on Biomedical Engineering*, vol. 56, no. 12, pp. 2858–2867, December 2009.

[7] A. Sixsmith and N. Johnson, "A smart sensor to detect the falls of the elderly," *IEEE Pervasive Computing*, vol. 3, no. 2, pp. 42–47, April 2004.

[8] D. Anderson, R.H. Luke, J.M. Keller, M. Skubic, M. Rantz, and M. Aud, "Linguistic summarization of video for fall detection using voxel person and fuzzy logic," *Computer Vision and Image Understanding*, vol. 113, no. 1, pp. 80–89, January 2009.

[9] L. Liu, M. Popescu, K.C. Ho, M. Skubic, and M. Rantz, "Doppler radar sensor positioning in a fall detection system," in *Proceedings of 2012 Annual International Conference of the IEEE Engineering in Medicine and Biology Society (EMBC)*, San Diego, CA, August 2012, pp. 256–259.

[10] P. Karsmakers, T. Croonenborghs, M. Mercuri, D. Schreurs, and P. Leroux, "Automatic in-door fall detection based on microwave radar measurements," in *Proceedings of 2012 9th European Radar Conference (EuRAD)*, Amsterdam, Netherland, October 2012, pp. 202–205.

[11] M. Wu, X. Dai, Y. D. Zhang, B. Davidson, J. Zhang, and M. G. Amin, "Fall detection based on sequential modeling of radar signal time-frequency features," in *Poceedings of IEEE International Conference on Healthcare Informatics*, Philadelphia, PA, September 2013, pp. 169–174.

[12] M.G. Amin, Y.D. Zhang, F. Ahmad, and K.C. Ho, "Radar signal processing for elderly fall detection," *IEEE Signal Processing Magazine*, (in press).

[13] Y. Kim and H. Ling, "Human activity classification based on micro-Doppler signatures using a support vector machine," *IEEE Transactions on Geoscience and Remote Sensing*, vol. 47, no. 5, pp. 1328–1337, May 2009.

[14] Q. Wu, Y.D. Zhang, W. Tao, and M.G. Amin, "Radar-based fall detection based on Doppler time-frequency signatures for assisted living," *IET Radar, Sonar & Navigation*, vol. 9, no. 2, pp. 164–172, February 2015.

[15] A. Gadde, M.G. Amin, Y.D. Zhang, and F. Ahmad, "Fall detection and classification based on time-scale radar signal characteristics," in *Poceedings of SPIE, vol. 9077*, Baltimore, MD, May 2014, pp. 1–9.

[16] B.-Y. Su, K.C. Ho, M.J. Rantz, and M. Skubic, "Doppler radar fall activity detection using the wavelet transform," in *IEEE Transactions on Biomedical Engineering*, March 2014, vol. 62, pp. 865–875.

[17] L.B. Almeida, "The fractional Fourier transform and time-frequency representations," *IEEE Transactions on Signal Processing*, vol. 42, no. 11, pp. 3084–3091, November 1994.

[18] R. Tao, Y.-L. Li, and Y. Wang, "Short-time fractional Fourier transform and its applications," *IEEE Transactions on Signal Processing*, vol. 58, no. 5, pp. 2568–2580, May 2010.

[19] D.M.J. Cowell and S. Freear, "Separation of overlapping linear frequency modulated (LFM) signals using the fractional Fourier transform," *IEEE Transactions on Ultrasonics, Ferroelectrics, and Frequency Control*, vol. 57, no. 10, pp. 2324–2333, October 2010.

[20] X. Bai, R. Tao, L.-J. Liu, and J. Zhao, "Autofocusing of SAR images using STFRFT-based preprocessing," *Electronics Letters*, vol. 48, no. 25, pp. 1622–1624, December 2012.

[21] X. Chen, J. Guan, Z. Bao, and Y. He, "Detection and extraction of target with micromotion in spiky sea clutter via short-time fractional Fourier transform," *IEEE Transactions on Geoscience and Remote Sensing*, vol. 52, no. 2, pp. 1002–1018, February 2014.

[22] S.-H. Liu, T. Shan, Y.D. Zhang, R. Tao, and Y. Feng, "A fast algorithm for multi-component LFM signal analysis exploiting segmented DPT and SDFrFT," in *Proceedings of 2015 IEEE International Radar Conference (RadarCon)*, Arlington, VA, May 2015, pp. 1139–1143.

[23] S.-H. Liu, T. Shan, R. Tao, Y.D. Zhang, G. Zhang, F. Zhang, and Y. Wang, "Sparse discrete fractional Fourier transform and its applications," *IEEE Transactions on Signal Processing*, vol. 62, no. 24, pp. 6582–6595, December 2014.

[24] *Product Description: SDR-KIT 580*, Ancortek Inc., 2015, Available at http://ancortek.com/product/sdr-kit-580.